Journal of Power Sources 195 (2010) 1463–1471

Contents lists available at ScienceDirect

Journal of Power Sources

journal homepage: www.elsevier.com/locate/jpowsour

Chemical vapor synthesis and characterization of aluminum nanopowder

Jin Won Choi, Hong Yong Sohn*, Young Joon Choi, Zhigang Zak Fang

Department of Metallurgical Engineering, University of Utah, 135 South 1460 East, Room 412, Salt Lake City, UT 84112-0114, USA

ARTICLE INFO

Article history:
Received 23 July 2009
Received in revised form 1 September 2009
Accepted 2 September 2009
Available online 11 September 2009

Keywords:
Hydrogen storage
Chemical vapor synthesis
Aluminum nanopowder
Nanocrystalline materials

ABSTRACT

Aluminum is a component in many promising hydrogen storage materials such as aluminum hydride and complex aluminum hydrides. In this research, Al and $TiAl_3$-containing Al nanopowders were prepared by a chemical vapor synthesis (CVS) process using Mg as the reducing agent. XRD and EDS results indicated that the produced powder was composed of Al or Al with $TiAl_3$. The shape of the powder was spherical with the average size in the range of 10–50 nm measured by SEM, TEM, BET and ZetaPALS compared with the typically larger than 100 nm for commercially available fine Al powders. In addition, the effects of the operating conditions such as Ar flow rate, precursor feed rate and reaction temperature on the properties of the product powder were investigated.

1. Introduction

Hydrogen is one of the most promising alternative energy carriers [1,2]. Currently, the simplest and most common method of hydrogen storage uses thick-walled pressurized tanks. Other methods such as liquid hydrogen in a cryogenic tank, physisorption of hydrogen, metal hydrides and complex hydrides, many of them containing aluminum, as well as the use of hydrocarbons have been studied [1–6]. Metal hydrides and complex hydrides offer a safe way to store hydrogen. However, the kinetics of dehydrogenation is too slow in a near-ambient temperature and the reactions are not readily reversible under reasonable conditions [3,6]. To overcome these barriers, nanoparticles and doping elements are considered. Recent studies have shown that the dehydrogenation temperature can be lowered and the reversibility of hydrides such as sodium alanate can be increased by doping the compounds with Ti [7–9]. In addition, nanoscaled materials offer many advantages. The small size of these materials strongly enhances the kinetics of hydrogenation and dehydrogenation by increasing the reaction and diffusion rates. In other words, the reactivity per unit mass of nanostructured materials due to the large surface area is significantly higher and the diffusion path from surface to bulk is shorter than that of the larger sized materials.

The synthesis techniques for nanosized materials include gas condensation, plasma processing, chemical vapor synthesis (CVS), sol–gel, rapid quenching, crystallization of amorphous solids and mechanical milling/alloying [10,11]. Most methods require an extensive effort to control the size of the particles in the nanometer range to prevent agglomeration and oxidation due to the highly reactive nature of the particle surface. Chemical vapor synthesis is a method to prepare solid powders by vapor phase reactions. It was developed from the chemical vapor deposition technique to form particles instead of a film. CVS has considerable flexibility in producing nanomaterials by the use of a wide variety of precursors. The CVS process, which has been successfully developed at the University of Utah, involves reducing a vapor phase mixture of volatile precursors of the constituent metals by magnesium vapor or hydrogen, depending on the thermodynamics of the synthesis reactions. The key advantages of this process are the small size of produced particles, the ability to produce powders of many different compositions, the homogeneity of powder composition, and the ease of doping element addition in one-step synthesis. Sohn et al. [12–15] applied the basic concepts of the hydrogen reduction of metal chlorides to the CVS of intermetallic and metal alloy powders. When hydrogen is used, these chemical vapor reactions can generally be written as follows:

$$mMCl_x(g) + nNCl_y(g) + 0.5(mx + ny)H_2 = M_mN_n(s) + (mn + ny)HCl(g) \quad (1)$$

where M and N represent two different metals with x and y being the valences and M_mN_n being the intermetallic compound formed. Another key feature of chemical vapor synthesis is that it allows the formation of doped or multi-component nanoparticles through the use of multiple precursors. Sohn et al. [16] synthesized WC–Co composite powder by reducing WCl_6 and $CoCl_2$ precursors. Choi et al. [17] prepared Mg nanoparticles doped with Ti in a vapor phase reaction, which showed superior hydrogen storage properties. Ehrman

* Corresponding author. Tel.: +1 801 581 5491; fax: +1 801 581 4937.
E-mail address: h.y.sohn@utah.edu (H.Y. Sohn).

0378-7753/$ – see front matter © 2009 Elsevier B.V. All rights reserved.
doi:10.1016/j.jpowsour.2009.09.007

et al. [18] produced NaCl-encapsulated Si particles by reacting $SiCl_4$ with sodium vapor.

For automotive application, hydrogen storage materials based on light metal hydrides have attracted much attention. Numerous aluminum-containing compounds such as $NaAlH_4$ [8,9], AlH_3 [19], $LiAlH_4$ [20] and $Mg(AlH_4)_2$ [21] have been identified to have high potential as hydrogen storage materials. This prompted our effort to develop nanosized aluminum powder. Aluminum hydride or alane, AlH_3, is potentially a highly attractive storage material due to its high mass hydrogen capacity of 10 wt.%. However, experiments on AlH_3 exhibited slow H_2 evolution rates below 150 °C. It is very difficult to regenerate the spent aluminum powder back to AlH_3 [22]. One of the most promising candidates up to date is the aluminum based complex hydride, $NaAlH_4$. Bogdanovic and Schwickardi [7] showed that $NaAlH_4$ can be made reversible at relatively low temperatures and pressures by adding titanium. Recently, Lu et al. [23] discovered a combined hydrogen storage system of Li_3AlH_6–$LiNH_2$ which has 7.3 wt.% hydrogen capacity. They showed that this system is nearly 100% reversible according to the following reaction:

$$Li_3AlH_6 + 3LiNH_2 \leftrightarrow Al + 3Li_2NH + 4.5H_2 \quad (2)$$

Magnesium alanate, $Mg(AlH_4)_2$, is another attractive complex hydride, which has a theoretical hydrogen storage capacity of 9.3 wt.%. Researchers [24–28] have shown that it decomposes in two major steps according to the following reactions:

$$Mg(AlH_4)_2 \rightarrow MgH_2 + 2Al + 3H_2 \quad (3)$$

$$MgH_2 \rightarrow Mg + H_2 \quad (4)$$

$$2Al + Mg \rightarrow 1/2Al_2Mg_3 + 1/2Al \quad (5)$$

Despite the significant research on the hydrogenation behavior of the aluminum and complex aluminum hydrides, little information is available on the aluminum nanopowder as a starting material for the hydrogen storage materials. Light metal alloys are difficult to mill due to their ductility and reactivity. Therefore, in this research, an investigation was carried out on the synthesis of Al and $TiAl_3$-containing Al nanopowders from metal chlorides. More specifically, this research had the following goals: (1) chemical vapor synthesis of Al nanopowder using the Mg vapor reduction method and characterization of the product powder, (2) investigation of the effect of operating conditions on the nanosized powder production, (3) synthesis of intermetallic compound $TiAl_3$ as a dopant for the Al nanopowder.

2. Experimental apparatuses and procedures

2.1. Raw materials

The most commonly used reactants are metal chlorides, because of their high vapor pressures and purities. The chemicals $AlCl_3$, $TiCl_3$ and Mg powder were purchased from Sigma–Aldrich Chemical Co. The purity of the purchased reagent grade $AlCl_3$ was 98% and $TiCl_3$ was 99.99% pure. The particle size of the Mg powder was 177–420 μm (40–80 mesh) with 99.6% purity. Ultra high purity Argon (99.999%) was used to deliver the raw materials in an inert atmosphere.

To remove unwanted byproduct $MgCl_2$ from the collected powder, 200 proof pure ethanol was used to prevent oxidation during rinsing (anhydrous, ≥99.5%). For the collection of the powder, Anopore® inorganic membrane with pore size of 20 nm was used for rinsing.

2.2. Preliminary experimental apparatus

Preliminary experiments were conducted to examine the possibility of synthesizing Al powder by the proposed system [29]. Electrically heated reactor systems were used, each of which consisted of a horizontal or vertical tubular reactor, a volatilizer, a powder collector and an off-gas scrubber. In the earlier preliminary experiments, $AlCl_3$ was volatilized in an external volatilizer and Mg was volatilized from a ceramic boat placed inside the horizontal 316 stainless steel reactor tube. In the latter preliminary tests in a vertical alumina reactor, fine powders of the reactants $AlCl_3$ and Mg were fed into small alumina tubes placed in the top part of the reactor, which served as the volatilizers. The product powder was collected in a collector containing ethanol and the off-gas was neutralized by a NaOH solution. After the experiments, the collected powder was rinsed with 200 proof ethanol to remove unreacted $AlCl_3$ and the $MgCl_2$ produced from the reaction and then filtered by means of a filter with a pore size of 100 nm (anhydrous, ≥99.5%). Additional details can be found elsewhere [29].

The size, morphology and chemical composition of the powders were investigated with SEM (TOPCON SM-300), EDS and TEM (FEI Tecnai 30). The product powder was analyzed by XRD (Siemens D 5000) to identify the phase and calculate the average grain size of powder. The particle size distribution was measured by using a Brookhaven Instruments ZetaPALS unit which has a spatial resolution of 1 nm. ZetaPALS measures particle sizes based on the degree of spectral broadening induced in an incident laser beam by scattering from particles in a Brownian motion. The powder was suspended and diluted with pure ethanol in a vial. The vial was sonicated in an ultrasonic bath for 30 min to minimize agglomeration of the powder.

2.3. Improved experimental apparatus

The system was subsequently modified to obtain finer nano grains with a more uniform size distribution and increase the yield of the product by minimizing the buoyancy effect of the gas phase by using a horizontal reactor. Fig. 1(a) shows the modified CVS system. The diameter of the reactor was 5 cm and a graphite funnel was installed inside the reactor to enhance the mixing of the vaporized reactants. The system was composed of external entrained-flow powder feeders, reactor with volatilizer tubes and powder collecting system. The volatilizers were alumina tubes that extended into the mid-part of the reactor. Each precursor was placed in a glass tube, which was then mounted onto the powder feeder. Argon gas, shown by streams a and b in Fig. 1(b), was flowed through the powder feeder to act as a carrier for the precursor as well as to maintain an inert environment. At the same time, the glass tube was gradually pushed upward a desired rate by the syringe pump to feed the powder into the volatilizer. Calibration of the powder feeder indicated that a constant feed rate was maintained from the beginning until all the powder was discharged. The flow rate of the carrier Ar was 1 L min^{-1} in each stream. Additional carrier Ar with a flow rate of 0.3 L min^{-1} was supplied to prevent precursor from sticking in the feed tubes. These flow rates were kept the same for different runs because they were the optimum rates for the feeding of the precursors into the reactor. Dilution Ar gas shown as stream e in Fig. 1(b), was directly supplied into the reactor with various flow rates to control the gaseous reactant concentration. The total Ar flow rate was defined as the sum of all the flow rates (carrier, additional carrier and dilution Ar flow rates) to the reactor. The graphite funnel as shown in Fig. 1(c) was placed at 10 cm behind from the alumina feeding tubes for precursors to increase gas phase mixing. An alumina tube, 0.6 cm inner diameter, was connected to the graphite funnel to improve the mixing of gaseous reactants.

$AlCl_3$ and Mg precursors were filled in 1.3 and 1 cm diameter vial tubes, respectively, in the glove box and the weights of the vials were measured. During heating of the furnace to the target temperature, Ar gas was supplied into the reactor to remove residual oxygen and maintain an inert atmosphere. When the target tem-

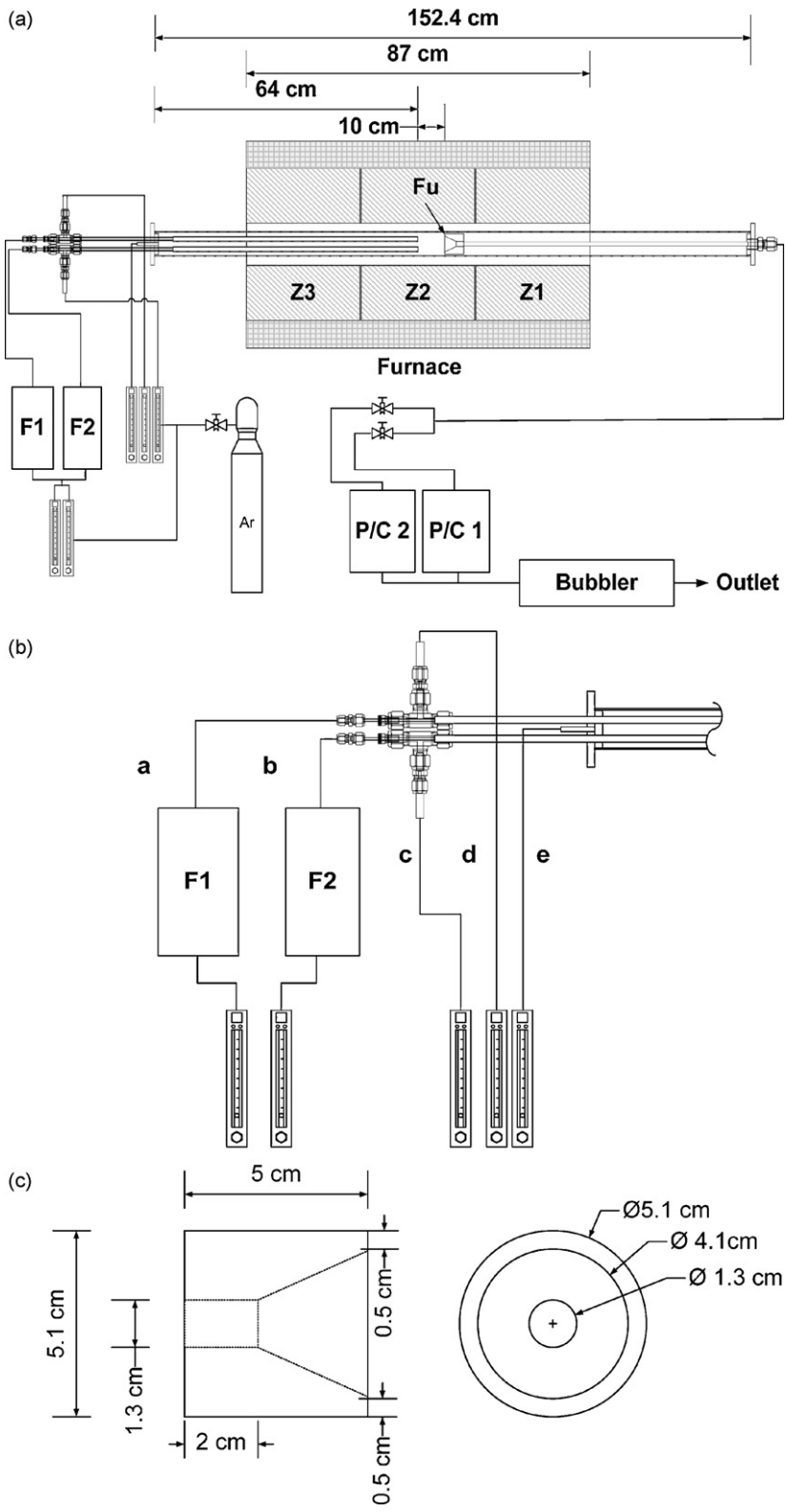

Fig. 1. (a) Modified horizontal experimental apparatus (F1, 2: entrained-flow powder feeders, Fu: Graphite funnel, Z1, 2, 3: Hot zones, P/C1, 2: powder collectors), (b) detailed view of the Ar inlet area (a and b: carrier Ar; c and d: additional carrier Ar; e: dilution Ar), and (c) detailed view of the graphite funnel.

perature was reached, the vials filled with precursors were placed in the powder feeders and the feeding rates were set according to the experimental conditions. Also, the Ar gas flow for precursor delivery and the dilution Ar flow were set for the experiments. When Ti-doped Al powder was to be synthesized, a small amount of $TiCl_3$ particles were added to $AlCl_3$ and the two components were uniformly mixed using a mortar and pestle to be fed into the reactor. Before collecting the produced powder, the off-gas/particle mix-

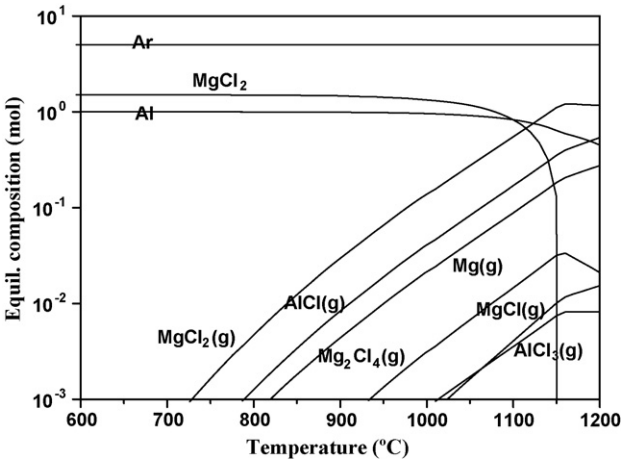

Fig. 2. Equilibrium composition vs. temperature for a mixture of 1 mol $AlCl_3$–1.5 mol Mg–5 mol Ar under 101.3 kPa pressure.

ture was passed through the bypass line for 5 min to stabilize the system. After stabilization, the produced powder was collected in the main filter and the off-gas from the filter was neutralized by a NaOH solution and vented.

3. Results and discussion

3.1. Equilibrium thermodynamics

Before starting any experiments, it is helpful to carry out a theoretical thermodynamic calculation to determine the conditions to produce the desirable phases. Equilibrium calculations were performed for the Al–Mg–Cl–Ar system under constant pressure. HSC Chemistry software version 5.1 [30], developed by Outokumpu Research Oy, which is based on the principle of the Gibbs free energy minimization, was used to calculate the thermodynamics of reactions. The thermodynamic data used for the calculation were taken from the HSC database. The calculation was performed under one atmospheric pressure and the effects of the experimental conditions were evaluated. Calculation of the equilibrium compositions was performed under one atmospheric pressure. The species considered in the equilibrium calculation were the gaseous species: Ar, $MgCl_2$, AlCl, Mg, Mg_2Cl_4, MgCl, $AlCl_3$, $AlCl_2$, MgCl, and Al plus the condensed phases: $MgCl_2$, Al, $AlCl_3$, and Mg. Apart from these species, other species such as Al_2Cl_6 and Al_2Cl_4 were considered in the preliminary calculations, but they were found to be present in negligible amounts in the range of conditions examined in this work.

Fig. 2 shows the equilibrium composition as a function of temperature. Al powder synthesis with the precursors is feasible over a wide temperature range. $MgCl_2$ is present as condensed phases below about 1100 °C because of its high boiling point, 1412 °C. As the temperature increases up to 1200 °C, the amounts of AlCl(g) and Mg(g) increase while the produced Al decreases. Although not shown in this figure, Al_3Mg_2 and $Al_{12}Mg_{17}$ are known to occur below 450 °C in the phase diagram of the Al–Mg system [31]. To prevent the formation of the intermetallic phases, the product must be quenched rapidly.

It is seen that in the temperature range considered the reaction can be represented by

$$AlCl_3(g) + 1.5Mg(g) = Al + 1.5MgCl_2(g) \quad (6)$$

The ΔG value of the reaction at 1000 °C is −29.2 kcal and the ΔH value at that temperature is −48.9 kcal.

3.2. Preliminary experiments

The aluminum powder synthesized at 1000 °C in the early preliminary experiments using a 316 stainless steel reactor contained spherical particles of sizes between 200 nm and 2 μm. The EDS analysis showed that the particles were composed of Al, Mg and other impurities such as Fe, Cr and Mn. These impurities came from the stainless steel reactor by reacting with chlorides. The average grain size calculated from the XRD peaks by applying the Scherrer equation [32] was around 47 nm, which means that the particles consisted of several grains because the particle size was larger than the grain size. The wide distribution of size might be caused by the low feeding rate of total Ar. It was found that approximately half of the particles produced by the chemical reaction were deposited inside the reactor. The control of input precursor was very difficult because the amount of input materials was controlled by their vapor pressure. However, the feasibility of the Al synthesis was confirmed with these experiments.

A second set of preliminary experiments in a modified CVS system with a vertical alumina tube reactor yielded nano grained Al powder with higher purity. The shape of the powder was again spherical. The particle size was between 100 nm and 1 μm, which indicated that the particles were smaller and more uniform than those from the earlier preliminary experiments. The crystallite size calculated by the Scherrer's equation was 40 nm. The EDS analysis confirmed that the composition of the products was Al with negligible amounts of impurities found in the previous experiments. However, the produced particle size was still not in the nano range, although the grain size was 40 nm.

3.3. Main experiments

Although pure, nano grained Al powder was successfully synthesized with the second set of preliminary experiments, it was desired to obtain finer nano grains with a more uniform size distribution. Therefore, a new horizontal CVS system, shown in Fig. 1, was fabricated. Further, the horizontal system increased the product yield by reducing the loss on the wall caused by a buoyancy effect observed in the previous vertical apparatus. The experimental conditions were: reaction temperature of 1000 °C, evaporator temperatures of 1000 °C, $AlCl_3$ feeding rate of 0.1 g min^{-1}, Mg feeding rate of 0.03 g min^{-1} and dilution Ar flow rate of 9.85 L min^{-1}. The concentrations in the gas phase in the reactor were controlled by the dilution Ar flow. Under these conditions, the input molar ratio of $Mg/AlCl_3$ was 1.4–1.6. Fig. 3(a) and (b) shows, respectively, the SEM micrograph and chemical composition of the synthesized powder. Only Al was detected and there was no indication of other impurities in the EDS analysis. It is seen that the product powder was significantly agglomerated because of the fineness of the particles. Thus, TEM analysis was performed by diluting and sonicating the product powder in pure ethanol and using a Cu grid. The TEM micrograph of the dispersed powder in Fig. 4 indicates a spherical particle shape with sizes in the range of 10–50 nm. The particles were much smaller and more uniform than those from the previous experiments.

Fig. 5 shows XRD patterns of the sample before and after rinsing the product powder, with the rinsed sample on the lower pattern displaying only Al peaks, which indicates that the impurity problem encountered when stainless steel was used in the preliminary experiments was resolved. Based on the XRD and EDS analysis, it was concluded that sufficiently pure Al powder was synthesized successfully using the CVS system.

The particle size of the produced powder was also analyzed using the ZetaPALS unit. Each measurement was repeated three times and the results averaged. Fig. 6 presents the particle size distribution obtained. The average size was 17 nm with a narrow

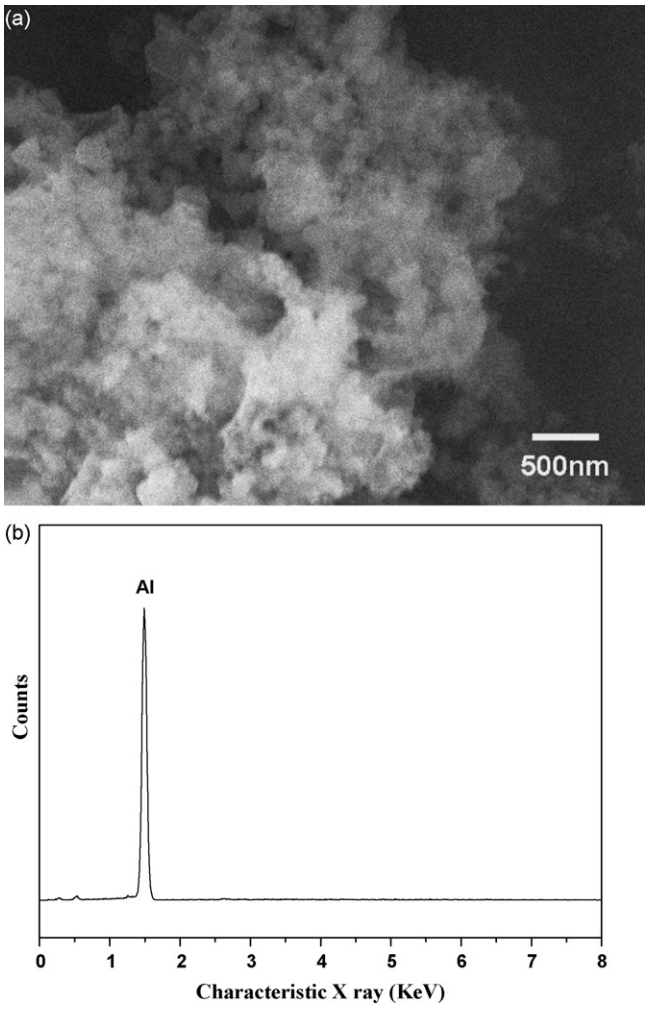

Fig. 3. (a) SEM micrograph and (b) EDS result of Al powder produced in the improved system.

distribution. The surface area of the particles was further measured using a BET surface area analyzer (ASAP 2100). The surface area was 103 $m^2\ g^{-1}$ corresponding to an average particle size of 22 nm. Thus, there was a good agreement among ZetaPALS, TEM and BET results in terms of the particle size.

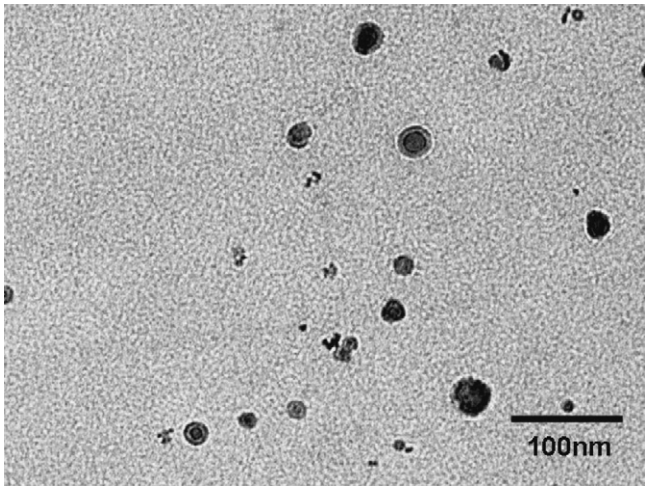

Fig. 4. TEM micrograph of Al powder produced in the improved system.

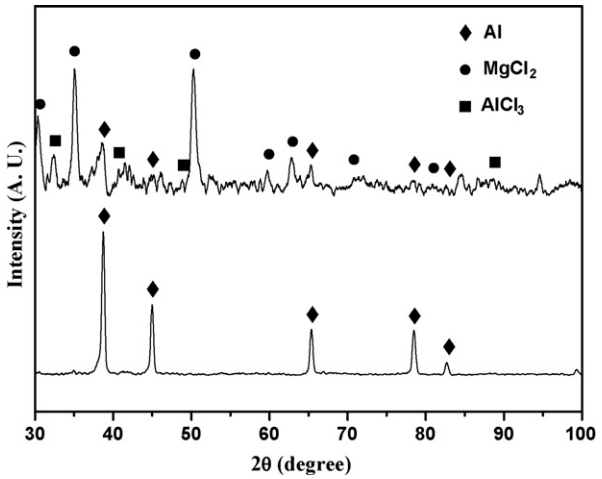

Fig. 5. XRD patterns of product Al powder (before and after rinsing with ethanol).

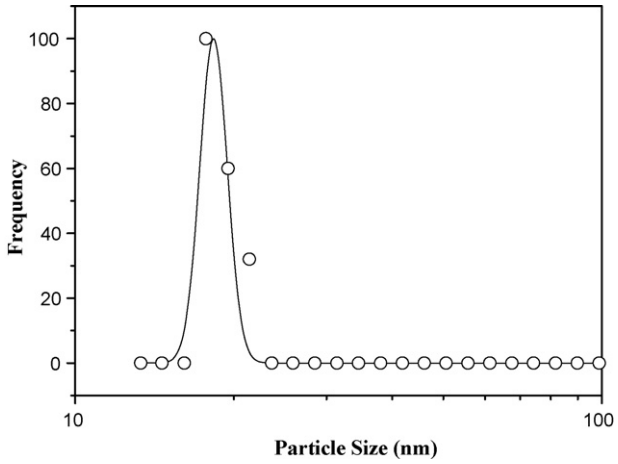

Fig. 6. ZetaPALS particle size analysis result of product Al powder.

The particle morphologies depend on the characteristic time of the collision and fusion. If the characteristic time for collision is much shorter than the characteristic time for fusion or sintering (e.g., $\tau_f/\tau_c > 10$), particle agglomeration will occur. If the characteristic time for collision is much longer than the characteristic time for fusion (e.g., $\tau_f/\tau_c < 0.1$) the particle will be spherical [33]. Accord-

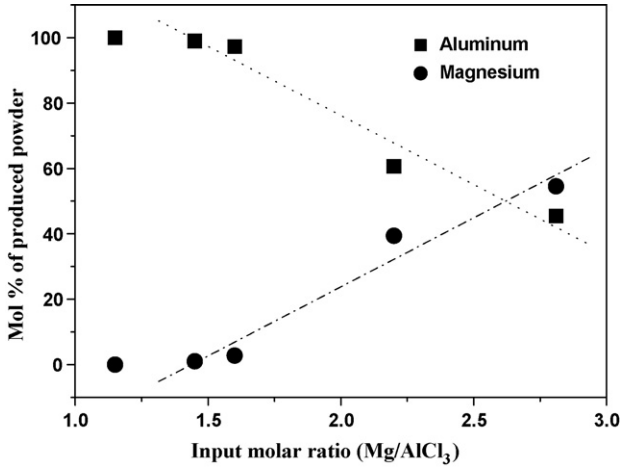

Fig. 7. Effect of Mg vapor supply on product composition.

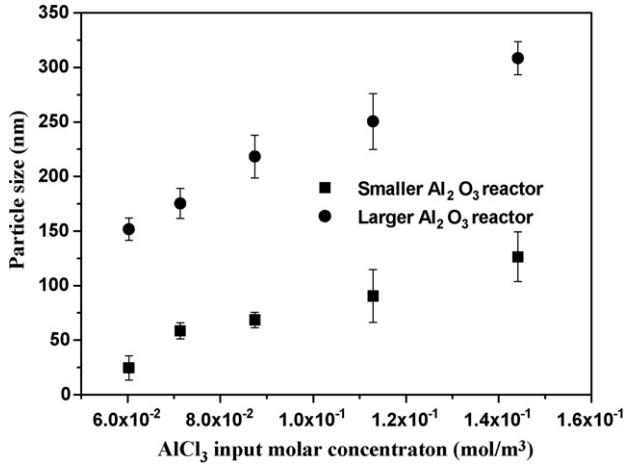

Fig. 8. The average particle size comparison of product Al powder (at 1000 °C, with various total Ar flow rates and different reactor diameters: 5 and 7.9 cm).

ing to the sintering of Al nanoparticles, the characteristic time for sintering is in the order of pico-seconds at 800 K [34]. Due to the fast characteristic time of sintering, spherical Al nanopowder was obtained in the CVS system. The particle size could be controlled by changing the total Ar flow rate based on the above results.

3.4. Effect of Mg vapor supply on Al formation

Aluminum has been found to destabilize MgH_2, and forms Mg/Al alloys upon dehydrogenation [35–39]. For example, Crivello et al. [39] reported that the Nb_2O_5 catalyzed Mg–Al alloys by ball milling process released 4.7 wt.% hydrogen under 250 °C. Thus, experiments were performed in this work to produce a mixture of Al and Mg by using various input ratios of $Mg/AlCl_3$. With an excess amount fed, the vaporized Mg served as both a reducing agent for $AlCl_3$ and a precursor for the Mg content in the product. The elemental compositions obtained from quantitative EDS analysis were plotted against the input ratio of $Mg/AlCl_3$. As shown in Fig. 7, the product was essentially pure Al until reaching the stoichiometric input molar ratio of 1.5. Beyond this ratio, the mole fraction of Al decreased proportionally with increasing Mg vapor supply. As expected from the phase diagram [31], intermetallic compound Al_3Mg_2 was formed by increasing the Mg input, which was confirmed by XRD analysis (not shown).

3.5. Effect of reactant concentration

The effect of reactant concentration on the Al particle synthesis was determined experimentally by changing the total Ar flow rate. Two alumina reactors with inner diameters of 7.9 and 5 cm were used to compare the particle size produced at different reactant concentration. The feed rates of the input precursor and reductant were kept the same ($AlCl_3$ feeding rate of 0.1 g min^{-1} and Mg feeding rate of 0.03 g min^{-1}). The dilution Ar flow rate was varied from 2.6 to 9.85 L min^{-1} and the corresponding total Ar flow rate was from 5.2 to 12.5 L min^{-1}. The size of produced Al particles was measured by ZetaPALS.

Fig. 8 shows the variation in the average particle size of product particles with the $AlCl_3$ concentration at 1000 °C while the input ratio $AlCl_3$/Mg was fixed. The size of the product increased with increasing $AlCl_3$ concentration. The particle size, formed in the larger reactor, was in the range of 320–160 nm while 130–25 nm in the smaller reactor. The linear velocities of the gas mixture in the larger and smaller reactors were 14.5 and 36.1 cm s^{-1}, respectively. The particle size decreased with increasing gas velocity. With increasing total Ar flow, the concentration of input species decreased in the reactor which indicated that the concentration of the species in the reactor affected the particle size. The increase of total Ar flow rate also reduced the length of time that the particles spent in the reactor and consequently led to the decrease of particle size. Since the input amounts of the precursors were fixed,

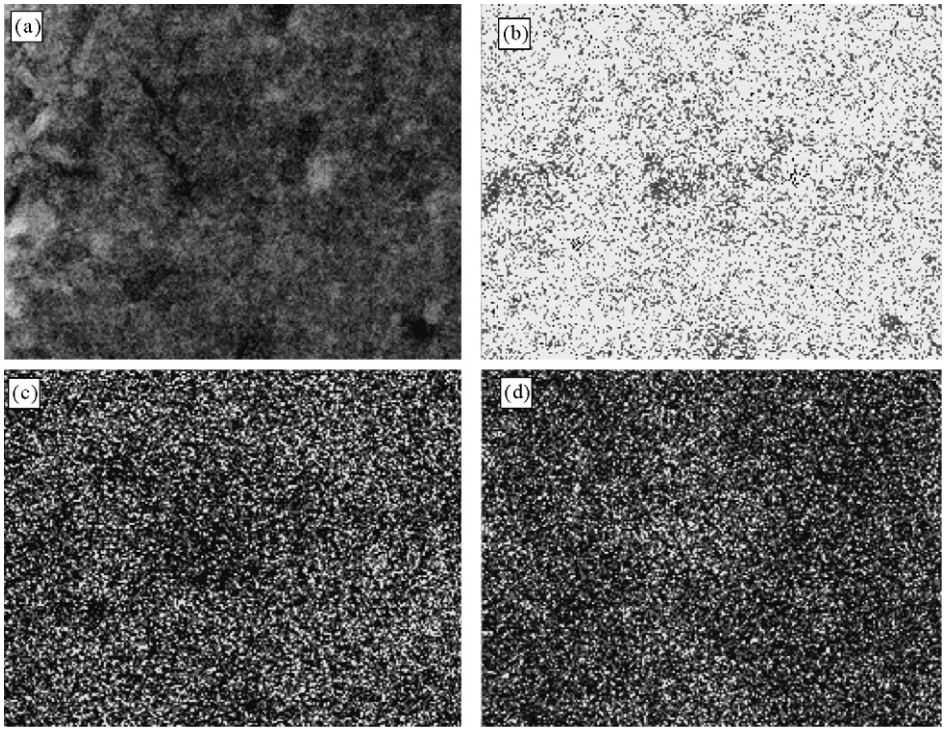

Fig. 9. EDS mapping results of the 4 mol% $TiCl_3$ doped Al powder (white regions indicate the elements). (a) SEM image of the powder, (b) Al, (c) Ti, and (d) Cl distribution map.

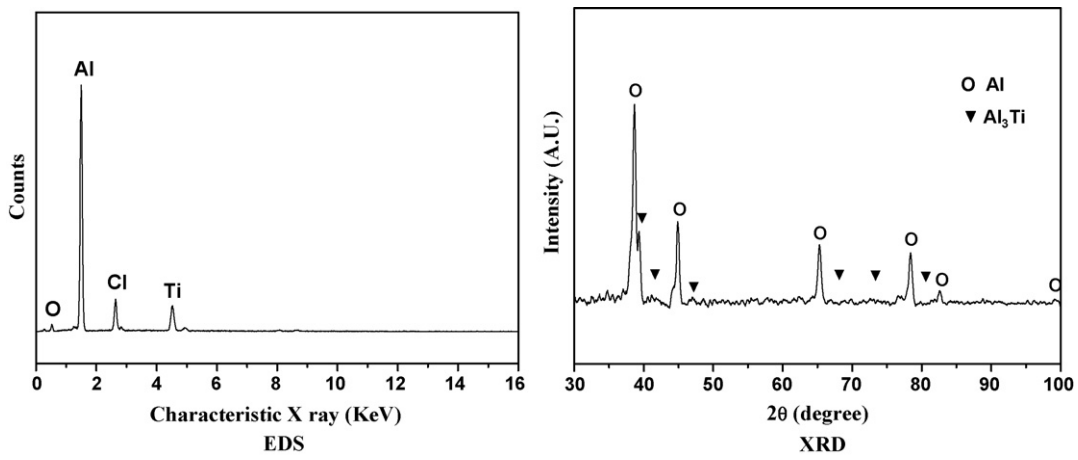

Fig. 10. EDS analysis and XRD patterns of the Al powder from the $AlCl_3$/4 mol% $TiCl_3$ mixture.

the concentration of gaseous species in the reactor decreased by increasing the total Ar flow rate. The lower concentration affects the nucleation of particles due to the lower ratio of supersaturation and slower growth of particle. The process of particle growth can be divided into the nucleation stage and the growth stage. During the nucleation stage, the vapor phase nucleation takes place as a series of addition of single molecule to develop into an embryo. This process introduces the formation of nucleus with a critical radius.

3.6. Synthesis of intermetallic compound $TiAl_3$ and Ti-doped Al nanopowder

As mentioned earlier, Ti doping increases the kinetics of dehydrogenation. Usually, Ti doping is done by milling, but it is difficult to mill Al powder due to its high ductility. In the CVS process, doping can be effected during the powder synthesis by directly mixing $TiCl_3$ with the precursors. To maximize the doping effect on the hydrogenation kinetics, uniform distribution of the dopant on the particle surface is important. To achieve these goals, two types of doping methods were used.

First, the dopant of 4 mol% $TiCl_3$ was premixed with the precursor $AlCl_3$. This percentage was based on the weight of $TiCl_3$ and $AlCl_3$, not including Mg. The input molar ratio of $AlCl_3$/Mg was 0.64 for the reduction of the mixture. The dilution Ar flow of the reactor was 9.85 L min^{-1} and the experimental temperature was 1000 °C. Fig. 9 shows the SEM image and EDS mapping results of the product powder. The dopant was uniformly distributed in the products. The EDS result in Fig. 10 shows that the CVS powder was composed of Al, Cl, Ti and a small amount of oxygen. The molar ratio Ti/Al in the product power was 0.06, based on the EDS quantitative analysis. The Ti mole fraction in the product was higher than in the feed. One of the possible reasons for this result is the higher $(-\Delta G^{\circ})$ value

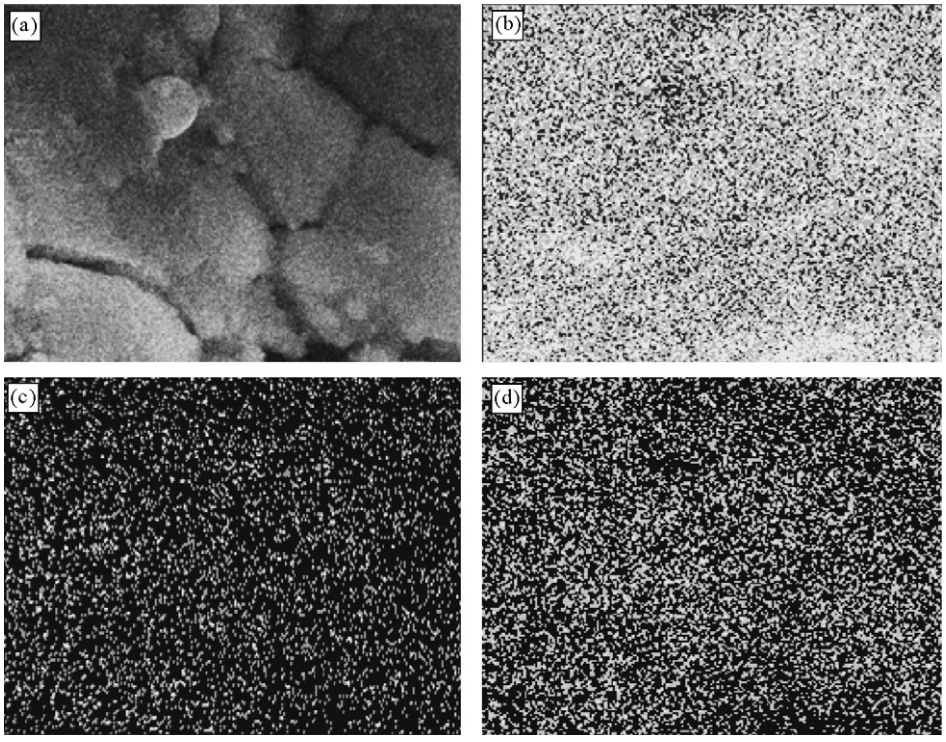

Fig. 11. EDS mapping of the liquid phase $TiCl_3$ doped Al powder (white regions indicate the elements). (a) SEM image of the powder, (b) Al, (c) Ti, and (d) Cl distribution map.

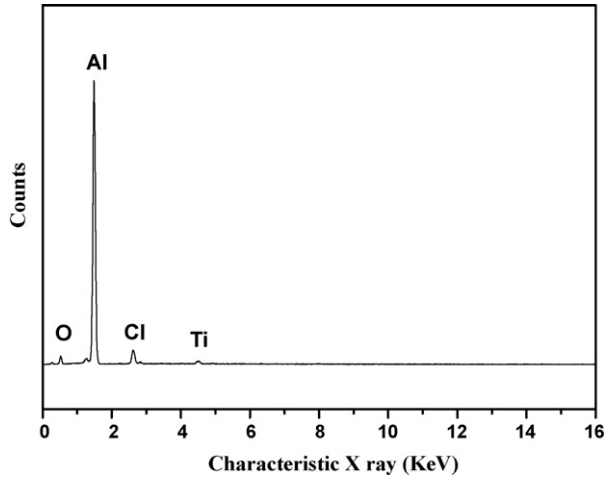

Fig. 12. EDS analysis of the liquid phase Ti-doped CVS Al powder.

of the reaction between Mg and $TiCl_3$ (−34.82 kcal at 1000 °C) than that of the reaction between Mg and $AlCl_3$ (−26.11 kcal at 1000 °C). Thus, $TiCl_3$ was preferentially reduced by the Mg vapor in the reactor. The XRD pattern in Fig. 10 shows that intermetallic compound $TiAl_3$ was formed due to the reaction between the reduced Al and Ti. The ΔG° of the $TiAl_3$ formation at 1000 °C is $-24.8\,kcal\,mol^{-1}$, which makes the reaction feasible.

Second, liquid phase doping was applied for the CVS Al powder because this method provides another efficient way for doping the material on the particle surface. 4 mol% $TiCl_3$ dissolved in ethanol was applied on the Al CVS powder and dried. The process was performed in the glove box to prevent oxidation. Fig. 11 shows the results of EDS mapping. $TiCl_3$ was uniformly distributed on the product powder. Fig. 12 shows the EDS elemental analysis of the liquid phase doping. The products contained 1.04 at.% Ti while the amount of Cl was 5.45 at.% based on the EDS quantitative analysis. The results of the first method showed that the product contained $TiAl_3$ while the second method did not produce the intermetallic compound. In the second method, the doping process was done at room temperature and thus the resulting product did not contain the intermetallic compound.

It has been reported that the intermetallic compound $TiAl_3$ formed during the high temperature processing also acts as a dopant [8,40–42]. Researchers [8,40,41] have confirmed that during the milling process of $NaAlH_4$ with 4 mol% $TiCl_3$, $TiAl_3$ can be formed by a mechanochemical reaction in the mixed powder and the kinetics of dehydrogenation and hydrogen kinetics was improved due to the uniform distribution of the intermetallic compound. Kang et al. [42] demonstrated the catalytic effect of $TiAl_3$ on $NaAlH_4$. Therefore, both methods can be applied to the preparation of Ti-doped Al powder for the hydrogen storage applications. It is planned in this laboratory to investigate the full potential of Ti-doped nanosized Al on $NaAlH_4$ to better understand the thermodynamics and kinetics of the reaction.

4. Conclusions

In the present work, a CVS technique was applied to the preparation of nanosized Al powder using a horizontal furnace and external feeding system, which has several advantages. First, it is a combined unit which has a volatilization system and a reaction system inside the reactor. Second, a powder feeding system was designed for an accurate control of the precursors. The precursor was supplied by the powder feeder which was operated pneumatically to feed fine solid particles directly into the reactor at constant rates. Using this CVS system, Al and $TiAl_3$-containing Al were synthesized. Pure Al nanoparticle of ~20 nm was successfully obtained, and Ti doping was effectively applied on the Al nanopowder using premixed precursors. EDS analysis confirmed that the Ti was uniformly distributed with the produced Al. Finally, the CVS system has been proved to be capable of producing various nanosized particles with narrow size distributions by using different precursors.

Acknowledgements

This material is based upon work supported in part by the University of Utah Funding Incentive Seed Grant Committee and the U.S. DOE Metal Hydride Center of Excellence under contract number DE-FC36-05GO15069. One of the authors (JWC) acknowledges financial support from Korean Air Force toward his work for a Ph.D. degree.

References

[1] C.J. Winter, J. Nitsch, Hydrogen as an Energy Carrier: Technologies, Systems Economy, Springer-Verlag, Berlin, New York, 1988, pp. 16–28.
[2] N.N. Greenwood, A. Earnshaw, Chemistry of the Elements, second ed., Butterworth-Heinemann, Oxford (England), Boston, 1998, pp. 32–64.
[3] L. Schlapbach, A. Züttel, Nature 414 (2001) 353–358.
[4] A. Züttel, Mater. Today 6 (2003) 24–33.
[5] A. Züttel, Naturwissenschaften 91 (2004) 157–172.
[6] G. Sandi, Interface 13 (2004) 40–44.
[7] B. Bogdanovic, M. Schwickardi, J. Alloys Compd. 253–254 (1997) 1–9.
[8] C.M. Jensen, R. Zidan, N. Mariels, A. Hee, C. Hagen, Int. J. Hydrogen. Energy 24 (1999) 461–465.
[9] J. Iniguez, T. Yildirim, Appl. Phys. Lett. 86 (2005), 103109_1-193109_3.
[10] C. Suryanarayana, Prog. Mater. Sci. 46 (2001) 1–184.
[11] M.T. Swihart, Curr. Opin. Colloid Interface Sci. 8 (2003) 127–133.
[12] H.Y. Sohn, S. Paldey, J. Mater. Res. 13 (1998) 3060–3069.
[13] H.Y. Sohn, S. Paldey, Mater. Sci. Eng. A, Struct. Mater. Prop. Microstruct. Process. 247 (1998) 165–172.
[14] H.Y. Sohn, S. Paldey, Metall. Mater. Trans. B, Proc. Metall. Mater. Proc. Sci. 29 (1998) 457–464.
[15] H.Y. Sohn, S. Paldey, Metall. Mater. Trans. B, Proc. Metall. Mater. Proc. Sci. 29 (1998) 465–469.
[16] H.Y. Sohn, T. Ryu, J.W. Choi, K.S. Hwang, G. Han, Y.J. Choi, Z.Z. Fang, JOM 59 (12) (2007) 44–49.
[17] Y.J. Choi, J.W. Choi, H.Y. Sohn, T. Ryu, K.S. Hwang, Z.Z. Fang, Int. J. Hydrogen Energy 34 (2009) 7700–7706.
[18] S.H. Ehrman, M.I. Aquino-Class, M.R. Zachariah, J. Mater. Res. 14 (1999) 1664–1671.
[19] G. Sandrock, J. Reilly, J. Graetz, W.-M. Zhou, J. Johnson, J. Wegrzyn, J. Alloys Compd. 421 (2006) 185–189.
[20] V.P. Balema, K.W. Dennis, V.K. Pecharsky, Chem. Commun. 17 (2000) 1665–1666.
[21] M. Fichtner, O. Fuhr, J. Alloys Compd. 345 (2002) 286–296.
[22] J. Graetz, J.J. Reilly, J. Phys. Chem. B 109 (2005) 22181–22185.
[23] J. Lu, Z.Z. Fang, H.Y. Sohn, J. Phys. Chem. B 110 (2006) 14236–14239.
[24] M. Fichtner, O. Fuhr, O. Kircher, J. Alloys Compd. 356–357 (2003) 418–422.
[25] A. Fossdal, H.W. Brinks, M. Fichtner, B.C. Hauback, J. Alloys Compd. 404–406 (2005) 752–756.
[26] R. Gremaud, A. Borgschulte, W. Lohstroh, H. Schreuders, A. Züttel, B. Dam, R. Griessen, J. Alloys Compd. 404–406 (2005) 775–778.
[27] Y. Kim, E.-K. Lee, J.-H. Shim, Y.W. Cho, K.B. Yoon, J. Alloys Compd. 422 (2006) 283–287.
[28] K. Komiya, N. Morisaku, Y. Shinzato, K. Ikeda, S. Orimo, Y. Ohki, K. Tatsumi, H. Yukawa, M. Morinaga, J. Alloys Compd. 446–447 (2007) 237–241.
[29] J.W. Choi, Chemical vapor synthesis and characterization of metallic nanopowders relevant to hydrogen storage materials, Ph.D. dissertation, University of Utah, Salt Lake City, Utah, 2009.
[30] HSC Chemistry, Version 5.1, Outokumpu Research Oy, Finland, 2002.
[31] A.S.M. International, ASM Handbook, Alloy Phase Diagrams, ASM International, Materials Park, OH, 1992, pp. 2–48, 2–282.
[32] H.P. Klug, L.E. Alexander, X-ray Diffraction Procedures for Polycrystalline and Amorphous Materials, second ed., John Wiley & Sons, New York, 1974, p. 156.
[33] T.T. Kodas, M.J. Hampden-Smith, Aerosol Processing of Materials, Wiley-VCH, New York, 1999, pp. 97–100, 124–127.
[34] J.S. Raut, R.B. Bhagat, K.A. Fichthorn, Nanostruct. Mater. 10 (1998) 837–851.
[35] S. Bouaricha, J.P. Dodelet, D. Guay, J. Huot, S. Boily, R. Schulz, J. Alloys Compd. 297 (2000) 282–293.
[36] A. Zaluska, L. Zaluski, J.O. Ström-Olsen, Appl. Phys. A, Mater. Sci. Process. 72 (2001) 157–165.

[37] J.-C. Crivello, T. Nobuki, S. Kato, M. Abe, T. Kuji, J. Alloys Compd. 446–447 (2007) 157–161.
[38] A. Andreasen, Int. J. Hydrogen Energy 33 (2008) 7489–7497.
[39] J.-C. Crivello, T. Nobuki, T. Kuji, Int. J. Hydrogen Energy 34 (2009) 1937–1943.
[40] B. Bogdanovic, M. Felderhoff, M. Germann, M. Härtel, A. Pommerin, F. Schüth, C. Weidenthaler, B. Zibrowius, J. Alloys Compd. 350 (2003) 246–255.
[41] D.D. Graham, L.F. Culnane, M. Sulic, C.M. Jensen, I.M. Robertson, J. Alloys Compd. 446–447 (2007) 255–259.
[42] X.D. Kang, P. Wang, X.P. Song, X.D. Yao, G.Q. Lu, H.M. Cheng, J. Alloys Compd. 424 (2006) 365–369.